Available online at www.sciencedirect.com
ScienceDirect
Journal of Sound and Vibration 317 (2008) 994–1016
JOURNAL OF SOUND AND VIBRATION
www.elsevier.com/locate/jsvi

An analytic Green's function for a lined circular duct containing uniform mean flow

Sjoerd W. Rienstra[a,*], Brian J. Tester[b]

[a]*Department of Mathematics & Computer Science, Eindhoven University of Technology, P.O. Box 513, 5600 MB Eindhoven, The Netherlands*
[b]*Institute of Sound and Vibration Research, University of Southampton, Highfield, Southampton S017 1BJ, UK*

Received 28 February 2006; received in revised form 21 March 2008; accepted 27 March 2008
Handling Editor: C.L. Morfey
Available online 9 June 2008

Abstract

An analytic Green's function is derived for a lined circular duct, both hollow and annular, containing uniform mean flow, from first principles by Fourier transformation. The derived result takes the form of a common mode series. We show that the analytic Green's function for a lined hollow circular duct, containing uniform mean flow, is essentially identical to that used by Tester et al. in the Cargill splice scattering model. The explicit form of the Green's function for the annular duct is new.

A more comprehensive causality analysis suggests the possibility of certain upstream modes being really downstream instabilities. As their growth rates are usually exceptionally large, including these modes as instabilities is both not practical and in disagreement with most (not all) experiments. Therefore, we outline the possibility but do not include them in the presented examples. We follow the "modelling assumption" that all modes decay in their respective direction of propagation.

To illustrate the advantages of our analytic result compared to the matrix inversion technique of Alonso et al., we compute the mode amplitudes from both methods for a typical aircraft engine intake condition. The comparisons show good agreement without flow, irrespective of how many modes are included in the matrix inversion for the numerical mode amplitudes. With flow, the mode amplitudes do not agree but as the number of modes included in the matrix inversion is increased, enough to include any important surface waves, the numerically obtained modal amplitudes of Alonso et al. appear to be converging to the present analytical result.

In practical applications our closed form analytic Green's function will be computationally more efficient, especially at high frequencies of practical interest to aero-engine applications, and the analytic form for the mode amplitudes could permit future modelling advances not possible from the numerical equivalent. It also may have application to post-processing of phased array measurements inside lined ducts.

*Corresponding author.
E-mail addresses: S.W.Rienstra@tue.nl (S.W. Rienstra), brian.j.tester@dsl.pipex.com (B.J. Tester).

0022-460X/$ - see front matter © 2008 Elsevier Ltd. All rights reserved.
doi:10.1016/j.jsv.2008.03.048

Nomenclature

a	duct diameter
$\mathscr{C}_m$, $\mathscr{D}_m$	linear combinations of Bessel functions J_m and Y_m
$\boldsymbol{e}_x$, $\boldsymbol{e}_r$, $\boldsymbol{e}_\theta$	unit vectors in x, r, θ-direction
E_m	auxiliary functions of κ
$F_m, H_m, \mathscr{F}_m, \mathscr{H}_m$	auxiliary functions of r and α
$G(\boldsymbol{x};\boldsymbol{x}_0)$	Green's function (in pressure)
$G_m(r,x)$	m-th circumferential Fourier component of $G(\boldsymbol{x};\boldsymbol{x}_0)$
$H(x)$	Heaviside step function
h	hub-tip ratio (dimensionless hub radius)
J_m, Y_m	Bessel functions of the first and second kinds of order m
m	circumferential modal order
M	Mach number
$\boldsymbol{n}$	unit outer normal vector at $r=1$
p, $\boldsymbol{v}$, ρ, c	time-harmonic pressure, velocity, density, sound speed
x, r, θ, t	axial, radial, azimuthal angle, time co-ordinate
Z_1, Z_h	impedance of outer, inner wall
α	radial modal wave number; (square root of minus) eigenvalue of Laplace operator
β	$(1-M^2)^{1/2}$
δ	parameter in numerical procedure
κ	axial wave number
μ	radial modal order
σ	reduced axial wave number
ω	Helmholtz number (dimensionless angular frequency)
ϖ	ω/β
Ω	$\omega-\kappa M$

1. Introduction

In some recent work, Tester et al. [1,2] described the development and validation of an analytical model for the scattering of spinning modes by liner splices, originally derived by Cargill [3] and based on the Kirchhoff approximation. In his original formulation, Cargill used the hard-walled radial eigenfunctions in the Green's function for a circular duct containing uniform flow. In the recent work [1] an analytic, closed form Green's function was used that was deduced from that given by Tester [4] for a lined 2D duct containing uniform flow. This was assumed to be an approximation although it can be shown that it is a special case of the result derived by Swinbanks [5] for a lined 2D duct containing sheared flow.

In his thesis [6], Schulten gave a version of the spatially Fourier-transformed Green's function of a lined annular duct, with the suggestion to invert this Fourier-transform expression numerically. No actual examples were given, however. Closer to our formulation is the work of Zorumski in Ref. [7]. Not all formulas are worked out explicitly and no details are given about the numerical evaluation and the role of surface waves. More recently Alonso et al. [8] have proposed an 'exact' Green's function based on the numerical inversion of a matrix, which has been evaluated in the course of the present work.

In the current work we derive an analytic Green's function for a lined circular duct, both hollow and annular, containing uniform mean flow, from first principles in closed form, and show that the hollow version is essentially identical to that used in Ref. [1].

Comparisons are presented with the 'numerical' Green's function of Alonso et al. [8,9]. In these presented examples we assumed that all modes decay in their respective direction of propagation, although more comprehensive causality analyses [4,10,11], supports the conjecture that some supposedly upstream-running modes are downstream-running convective instabilities (with the same harmonic time dependence as the exciting source). Moreover, recently Brambley et al. [12] showed that the liner-mean-flow system may be absolutely unstable, in which case any convective instability would be meaningless.

The conjectured unstable behaviour is, at least in the realm of the model, confirmed by numerical calculations in time-domain by Chevaugeon et al. [13]. The *physical* existence on the other hand is not so clear, but instabilities have been reported by Ronneberger et al. [14] and Aurégan et al. [15] in experiments with impedances of small resistance with predicted (convective) instabilities of small growth rate [10]. For most impedances met in practice, however (including the ones considered here) the predicted growth rates are exceptionally large, in which case their physical relevance is questionable as these instabilities have never been reported [16], and at the same time their inclusion is not practical. For this reason their role is not further

explored in the present study, but we will show that, if desired, any such modes may be easily included as a convective instability in the present format.

If the liner-mean-flow system is indeed absolutely unstable, including these modes is futile, and we have to search for other, stable models. At present, this is beyond the scope of our paper.

2. The problem

Consider a cylindrical duct of radius $a>0$ (possibly annular with inner radius ah), a mean flow of subsonic Mach number M, sound speed c_0 and density ρ_0 and harmonic pressure and velocity perturbations $\tilde{p}$ of angular frequency $\tilde{\omega}$ (see the sketch Fig. 1). We make dimensionless

$$\tilde{\boldsymbol{x}} = x a, \quad \tilde{t} = ta/c_0, \quad \tilde{\omega} = \omega c_0/a, \quad \tilde{p} = \rho_0 c_0^2 \,\mathrm{Re}(p\mathrm{e}^{\mathrm{i}\omega t}). \tag{1}$$

The Green function $G(\boldsymbol{x};\boldsymbol{x}_0)$ is represented by the pressure field $p(\boldsymbol{x})$ that is excited by a point source at $\boldsymbol{x}_0$, and satisfies the equation

$$\nabla^2 G - \left(\mathrm{i}\omega + M\frac{\partial}{\partial x}\right)^2 G = \delta(\boldsymbol{x}-\boldsymbol{x}_0). \tag{2}$$

Note that we use the

$$\mathrm{e}^{\mathrm{i}\omega t}\text{ -convention.} \tag{3}$$

The Ingard–Myers impedance boundary condition [17,18] with flow, a linear relation between pressure and velocity, becomes in terms of the pressure at $r=1$

$$\left(\mathrm{i}\omega + M\frac{\partial}{\partial x}\right)^2 G + \mathrm{i}\omega Z_1 \frac{\partial G}{\partial r} = 0 \quad \text{at } r=1. \tag{4}$$

For a hollow duct finiteness of G is assumed at $r=0$. For an annular duct we have at the inner wall $r=h$

$$\left(\mathrm{i}\omega + M\frac{\partial}{\partial x}\right)^2 G - \mathrm{i}\omega Z_h \frac{\partial G}{\partial r} = 0 \quad \text{at } r=h. \tag{5}$$

Finally, we adopt radiation conditions that says that we only accept solutions that radiate away from the source position $\boldsymbol{x}_0$.

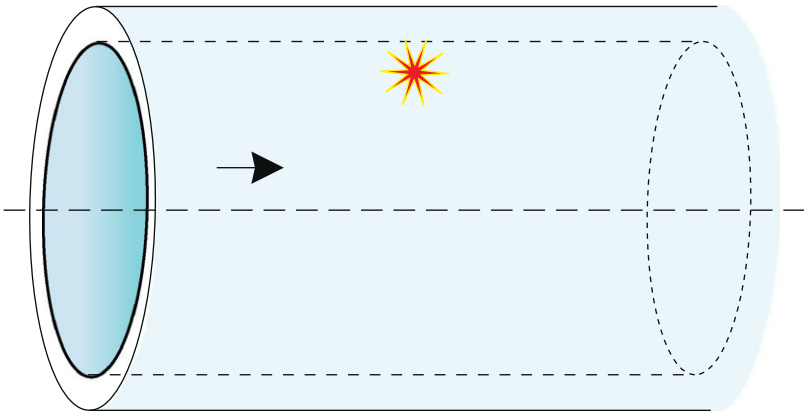

Fig. 1. Sketch of geometry: circular or annular lined duct with flow.

3. Solution

3.1. The hollow duct

We represent the delta-function by a generalised Fourier series in ϑ and Fourier integral in x

$$\delta(\boldsymbol{x}-\boldsymbol{x}_0)=\frac{\delta(r-r_0)}{r_0}\frac{1}{2\pi}\int_{-\infty}^{\infty}\mathrm{e}^{-\mathrm{i}\kappa(x-x_0)}\,\mathrm{d}\kappa\frac{1}{2\pi}\sum_{m=-\infty}^{\infty}\mathrm{e}^{-\mathrm{i}m(\vartheta-\vartheta_0)}. \tag{6}$$

where $0<r_0<1$, and write accordingly

$$G(x,r,\vartheta;x_0,r_0,\vartheta_0)=\sum_{m=-\infty}^{\infty}\mathrm{e}^{-\mathrm{i}m(\vartheta-\vartheta_0)}G_m(r,x)=\sum_{m=-\infty}^{\infty}\mathrm{e}^{-\mathrm{i}m(\vartheta-\vartheta_0)}\int_{-\infty}^{\infty}\hat{G}_m(r,\kappa)\mathrm{e}^{-\mathrm{i}\kappa(x-x_0)}\,\mathrm{d}\kappa. \tag{7}$$

Substitution of Eqs. (6) and (7) in Eq. (2) yields for $\hat{G}_m$

$$\frac{\partial^2\hat{G}_m}{\partial r^2}+\frac{1}{r}\frac{\partial\hat{G}_m}{\partial r}+\left(\alpha^2-\frac{m^2}{r^2}\right)\hat{G}_m=\frac{\delta(r-r_0)}{4\pi^2r_0}, \tag{8}$$

with

$$\alpha^2=\Omega^2-\kappa^2,\quad \Omega=\omega-\kappa M. \tag{9}$$

This has solution

$$\hat{G}_m(r,\kappa)=A(\kappa)J_m(\alpha r)+\frac{1}{8\pi}H(r-r_0)(J_m(\alpha r_0)Y_m(\alpha r)-Y_m(\alpha r_0)J_m(\alpha r)), \tag{10}$$

where J_m and Y_m denote the m-th order ordinary Bessel functions [19] of the first and second kind, $H(r-r_0)$ denotes the Heaviside stepfunction. Use is made of the Wronskian

$$J_m(x)Y_m'(x)-Y_m(x)J_m'(x)=\frac{2}{\pi x}. \tag{11}$$

A prime denotes a derivative to the argument, x. $A(\kappa)$ is to be determined from the boundary conditions at $r=1$, which is (assuming uniform convergence) per mode

$$\mathrm{i}\Omega^2\hat{G}_m+\omega Z_1\hat{G}_m'=0\quad\text{at } r=1. \tag{12}$$

A prime denotes a derivative to r. This yields

$$A=\frac{1}{8\pi}\left[Y_m(\alpha r_0)-\frac{\mathrm{i}\Omega^2Y_m(\alpha)+\omega\alpha Z_1Y_m'(\alpha)}{\mathrm{i}\Omega^2J_m(\alpha)+\omega\alpha Z_1J_m'(\alpha)}J_m(\alpha r_0)\right], \tag{13}$$

and thus

$$\hat{G}_m(r,\kappa)=J_m(\alpha r_<)\frac{\mathrm{i}\Omega^2F_m(r_>,\alpha)+\omega Z_1H_m(r_>,\alpha)}{8\pi E_m(\kappa)}, \tag{14}$$

where

$$E_m(\kappa)=\mathrm{i}\Omega^2J_m(\alpha)+\omega\alpha Z_1J_m'(\alpha), \tag{15a}$$

$$F_m(r,\alpha)=J_m(\alpha)Y_m(\alpha r)-Y_m(\alpha)J_m(\alpha r), \tag{15b}$$

$$H_m(r,\alpha)=\alpha J_m'(\alpha)Y_m(\alpha r)-\alpha Y_m'(\alpha)J_m(\alpha r), \tag{15c}$$

$$r_>=\max(r,r_0), \tag{15d}$$

$$r_<=\min(r,r_0). \tag{15e}$$

By substituting the defining series we find that F_m and H_m are analytic functions of α^2, while both E_m and $J_m(\alpha r_<)$ can be written as α^m times an analytic function of α^2. As a result, $\hat{G}_m(r,\kappa)$ is a meromorphic function of κ. It has isolated poles $\kappa=\kappa^{\pm}_{m\mu}$, given by $E_m(\kappa^{\pm}_{m\mu})=0$.

The final solution is found by Fourier back-transformation: close the integration contour around the lower half plane for $x>x_0$ to enclose the right propagating modes, and the upper half plane for $x<x_0$ to enclose the left propagating modes. We find

$$\left.\frac{\mathrm{d}E_m}{\mathrm{d}\kappa}\right|_{\kappa=\kappa_{m\mu}} = \omega Z_1 J_m(\alpha_{m\mu})\left[(\kappa_{m\mu}+\Omega_{m\mu}M)\left(1-\frac{m^2}{\alpha^2_{m\mu}}-\frac{\Omega^4_{m\mu}}{(\omega\alpha_{m\mu}Z_1)^2}\right)-\frac{2\mathrm{i}M\Omega_{m\mu}}{\omega Z_1}\right], \tag{16}$$

and introduce the quantity

$$Q^{\pm}_{m\mu} = \pm\left[(\kappa_{m\mu}+\Omega_{m\mu}M)\left(1-\frac{m^2}{\alpha^2_{m\mu}}-\frac{\Omega^4_{m\mu}}{(\omega\alpha_{m\mu}Z_1)^2}\right)-\frac{2\mathrm{i}M\Omega_{m\mu}}{\omega Z_1}\right], \tag{17}$$

where the $+,-$ signs apply to right, left-running modes. The integral is evaluated as a sum over the residues in the poles at $\kappa=\kappa^+_{m\mu}$ for $x>x_0$ and at $\kappa^-_{m\mu}$ for $x<x_0$, in short-hand notation given by

$$G_m(r,x) = -\frac{1}{4}\mathrm{i}\sum_{\mu=1}^{\infty} J_m(\alpha_{m\mu}r_<)\frac{\mathrm{i}\Omega^2_{m\mu}F_m(r_>,\alpha_{m\mu})+\omega Z_1 H_m(r_>,\alpha_{m\mu})}{\omega Z_1 Q_{m\mu}J_m(\alpha_{m\mu})}\mathrm{e}^{-\mathrm{i}\kappa_{m\mu}(x-x_0)}, \tag{18}$$

where $\alpha_{m\mu}=\alpha(\kappa_{m\mu})$. From eigenvalue equation $E_m(\kappa^{\pm}_{m\mu})=0$ and the Wronskian (11) we obtain

$$\begin{aligned}\mathrm{i}\Omega^2_{m\mu}F_m(r_>,\alpha_{m\mu})+\omega Z_1 H_m(r_>,\alpha_{m\mu}) &= -(\mathrm{i}\Omega^2_{m\mu}Y_m(\alpha_{m\mu})+\omega\alpha_{m\mu}Z_1 Y'_m(\alpha_{m\mu}))J_m(\alpha_{m\mu}r_>)\\ &= -\frac{2\omega Z_1}{\pi J_m(\alpha_{m\mu})}J_m(\alpha_{m\mu}r_>).\end{aligned} \tag{19}$$

So we can skip the distinction between $r_>$ and $r_<$ to achieve the soft wall modal expansion

$$G_m(r,x) = -\frac{1}{2\pi\mathrm{i}}\sum_{\mu=1}^{\infty}\frac{J_m(\alpha_{m\mu}r)J_m(\alpha_{m\mu}r_0)}{Q_{m\mu}J_m(\alpha_{m\mu})^2}\mathrm{e}^{-\mathrm{i}\kappa_{m\mu}(x-x_0)} = \sum_{\mu=1}^{\infty}G_{m\mu}(r)\mathrm{e}^{-\mathrm{i}\kappa_{m\mu}(x-x_0)}. \tag{20}$$

where for $x>x_0$ the sum pertains to the right-running waves, corresponding to the modal wave numbers $\kappa^+_{m\mu}$ found in the lower complex half plane, and for $x<x_0$ the left-running waves, corresponding to $\kappa^-_{m\mu}$ found in the upper complex half plane. Eq. (20) is essentially equivalent to Eq. (2) of Ref. [1] (see Appendix A).

Only if a mode from the upper half plane is to be interpreted as a right-running instability (see Refs. [4,10,20]), its contribution is to be excluded from the set of modes for $x<x_0$ and included in the modes for $x>x_0$. What we essentially do is deform the integration contour into the upper half plane, so the form of the solution remains exactly the same.

It may be noted that the solution is continuous everywhere, except at the source. As may be expected from the symmetry of the configuration, the clockwise and anti-clockwise rotating circumferential modes are equal, i.e. $G_m(r,x)=G_{-m}(r,x)$.

3.2. The annular duct

By choosing suitable variables we can make the solution for the annular duct similar to the one for the hollow duct. First we introduce two independent solutions of the scaled Bessel equation, i.e. the homogeneous version of Eq. (8), by

$$\mathscr{C}_m(r;\alpha) = aJ_m(\alpha r)+\ell Y_m(\alpha r), \tag{21a}$$

$$\mathscr{D}_m(r;\alpha) = cJ_m(\alpha r)+\mathscr{d}Y_m(\alpha r), \tag{21b}$$

where $ad \neq bc$ and $\mathscr{C}_m$ is supposed to satisfy the inner wall boundary condition, so a and b satisfy

$$\frac{b}{a} = -\frac{\mathrm{i}\Omega^2 J_m(\alpha h) - \alpha\omega Z_h J'_m(\alpha h)}{\mathrm{i}\Omega^2 Y_m(\alpha h) - \alpha\omega Z_h Y'_m(\alpha h)}. \tag{22}$$

Although not necessary for the final result, we will assume for convenience that $ad - bc = 1$ and

$$a = \mathrm{i}\Omega^2 Y_m(\alpha h) - \alpha\omega Z_h Y'_m(\alpha h), \quad b = -(\mathrm{i}\Omega^2 J_m(\alpha h) - \alpha\omega Z_h J'_m(\alpha h)).$$

$\mathscr{C}_m$ and $\mathscr{D}_m$ have now the Wronskian

$$\mathscr{C}_m\mathscr{D}'_m - \mathscr{D}_m\mathscr{C}'_m = (ad - bc)\frac{2}{\pi r} = \frac{2}{\pi r}. \tag{23}$$

The prime denotes a derivative to r. The solution of (8) that satisfies the inner wall boundary condition is

$$\hat{G}_m(r,\kappa) = A(\kappa)\mathscr{C}_m(\alpha r) + \frac{1}{8\pi}H(r - r_0)(\mathscr{C}_m(r_0;\alpha)\mathscr{D}_m(r;\alpha) - \mathscr{D}_m(r_0;\alpha)\mathscr{C}_m(r;\alpha)). \tag{24}$$

The boundary condition at $r = 1$ requires that A equals

$$A = \frac{1}{8\pi}\left[\mathscr{D}_m(r_0;\alpha) - \frac{\mathrm{i}\Omega^2\mathscr{D}_m(1;\alpha) + \omega Z_1\mathscr{D}'_m(1;\alpha)}{\mathrm{i}\Omega^2\mathscr{C}_m(1;\alpha) + \omega Z_1\mathscr{C}'_m(1;\alpha)}\mathscr{C}_m(r_0;\alpha)\right], \tag{25}$$

and thus

$$\hat{G}_m(r,\kappa) = \mathscr{C}_m(r_<;\alpha)\frac{\mathrm{i}\Omega^2\mathscr{F}_m(r_>,\alpha) + \omega Z_1\mathscr{H}_m(r_>,\alpha)}{8\pi\mathscr{E}_m(\kappa)}, \tag{26}$$

where

$$\mathscr{E}_m(\kappa) = \mathrm{i}\Omega^2\mathscr{C}_m(1;\alpha) + \omega Z_1\mathscr{C}'_m(1;\alpha), \tag{27a}$$

$$\mathscr{F}_m(r,\alpha) = \mathscr{C}_m(1;\alpha)\mathscr{D}_m(r;\alpha) - \mathscr{D}_m(1;\alpha)\mathscr{C}_m(r;\alpha), \tag{27b}$$

$$\mathscr{H}_m(r,\alpha) = \mathscr{C}'_m(1;\alpha)\mathscr{D}_m(r;\alpha) - \mathscr{D}'_m(1;\alpha)\mathscr{C}_m(r;\alpha). \tag{27c}$$

Note that Eq. (26) is the equivalent of Eq. (2.71), with Eqs. (2.43), (2.70) and (2.72), of Schulten [6]. Schulten suggested a numerical approach to evaluate the inverse Fourier transform, but did not give further details or examples.

In a similar way as with the hollow duct we can show that $\hat{G}_m$ is a meromorphic function in κ. Its Fourier integral that defines G_m can be evaluated in the form of a summation over the residues in $\kappa_{m\mu}$, the zeros of $\mathscr{E}_m(\kappa)$. From the defining relation $\mathscr{E}_m(\kappa_{m\mu}) = 0$ and the Wronskian we have at $\kappa = \kappa_{m\mu}$

$$\begin{aligned}\mathrm{i}\Omega^2\mathscr{F}_m(r_>;\alpha_{m\mu}) + \omega Z_1\mathscr{H}_m(r_>,\alpha_{m\mu}) &= -(\mathrm{i}\Omega^2\mathscr{D}_m(1;\alpha_{m\mu}) + \omega Z_1\mathscr{D}'_m(1;\alpha_{m\mu}))\mathscr{C}_m(r_>;\alpha_{m\mu})\\ &= -\frac{2\omega Z_1}{\pi\mathscr{C}_m(1;\alpha_{m\mu})}\mathscr{C}_m(r_>;\alpha_{m\mu}),\end{aligned}$$

and so we have the following result, which may be compared with equation (38), of Zorumski [7],

$$\begin{aligned}G_m(r,x) &= \int_{-\infty}^{\infty}\hat{G}_m(r,\kappa)\mathrm{e}^{-\mathrm{i}\kappa(x-x_0)}\,\mathrm{d}\kappa\\ &= -\frac{1}{2\pi\mathrm{i}}\mathrm{sign}(x - x_0)\sum_{\mu=1}^{\infty}\frac{\omega Z_1}{\mathscr{E}'(\kappa_{m\mu})}\frac{\mathscr{C}_m(r;\alpha_{m\mu})\mathscr{C}_m(r_0;\alpha_{m\mu})}{\mathscr{C}_m(1;\alpha_{m\mu})}\mathrm{e}^{-\mathrm{i}\kappa_{m\mu}(x-x_0)}.\end{aligned}$$

By carefully substituting definitions and Wronskians we obtain

$$\left[\frac{\mathrm{d}\mathscr{E}_m}{\mathrm{d}\kappa}\right]_{\kappa=\kappa_{m\mu}} = \omega Z_1\left[(\kappa_{m\mu}+\Omega_{m\mu}M)\left(1-\frac{m^2}{\alpha_{m\mu}^2}-\frac{\Omega_{m\mu}^4}{(\alpha_{m\mu}\omega Z_1)^2}\right)-\frac{2\mathrm{i}\Omega_{m\mu}M}{\omega Z_1}\right]\mathscr{C}_m(1;\alpha_{m\mu}) - \frac{2\omega Z_1}{\pi\mathscr{C}_m(1;\alpha_{m\mu})}\left[\mathscr{b}\frac{\mathrm{d}a}{\mathrm{d}\kappa}-a\frac{\mathrm{d}\mathscr{b}}{\mathrm{d}\kappa}\right]_{\kappa=\kappa_{m\mu}}.$$

Furthermore, we have

$$\left[\mathscr{b}\frac{\mathrm{d}a}{\mathrm{d}\kappa}-a\frac{\mathrm{d}\mathscr{b}}{\mathrm{d}\kappa}\right]_{\kappa=\kappa_{m\mu}} = \frac{2\omega^2 Z_h^2}{\pi}\left[(\kappa_{m\mu}+\Omega_{m\mu}M)\left(1-\frac{m^2}{\alpha_{m\mu}^2h^2}-\frac{\Omega_{m\mu}^4}{(\alpha_{m\mu}\omega Z_h)^2}\right)+\frac{2\mathrm{i}\Omega_{m\mu}M}{h\omega Z_h}\right], \tag{28}$$

and $\mathscr{C}_m(h;\alpha)=-2\omega Z_h/\pi h$. If we introduce

$$\mathscr{Q}_{m\mu}^{(1)\pm} = \pm\left[(\kappa_{m\mu}+\Omega_{m\mu}M)\left(1-\frac{m^2}{\alpha_{m\mu}^2}-\frac{\Omega_{m\mu}^4}{(\alpha_{m\mu}\omega Z_1)^2}\right)-\frac{2\mathrm{i}\Omega_{m\mu}M}{\omega Z_1}\right], \tag{29a}$$

$$\mathscr{Q}_{m\mu}^{(h)\pm} = \pm\left[(\kappa_{m\mu}+\Omega_{m\mu}M)\left(1-\frac{m^2}{\alpha_{m\mu}^2h^2}-\frac{\Omega_{m\mu}^4}{(\alpha_{m\mu}\omega Z_h)^2}\right)+\frac{2\mathrm{i}\Omega_{m\mu}M}{h\omega Z_h}\right] \tag{29b}$$

(again, the $\pm$ signs apply to right, left-running modes) we have finally in short-hand notation

$$G_m(r,x) = -\frac{1}{2\pi\mathrm{i}}\sum_{\mu=1}^{\infty}\frac{\mathscr{C}_m(r;\alpha_{m\mu})\mathscr{C}_m(r_0;\alpha_{m\mu})}{\mathscr{Q}_{m\mu}^{(1)}\mathscr{C}_m(1;\alpha_{m\mu})^2-h^2\mathscr{Q}_{m\mu}^{(h)}\mathscr{C}_m(h;\alpha_{m\mu})^2}\mathrm{e}^{-\mathrm{i}\kappa_{m\mu}(x-x_0)} = \sum_{\mu=1}^{\infty}G_{m\mu}(r)\mathrm{e}^{-\mathrm{i}\kappa_{m\mu}(x-x_0)}. \tag{30}$$

3.3. Lorentz-type or Prandtl–Glauert transformation

We obtain for hard walls some simplification by the following Lorentz-type or Prandtl–Glauert transformation. In this case the left and right-running values of $\alpha_{m\mu}$ are symmetric, i.e. $\alpha_{m\mu}^+=\alpha_{m\mu}^-$, while the corresponding values of $\kappa_{m\mu}$ are point symmetric in $-\omega M/(1-M^2)$. When we transform

$$\beta=\sqrt{1-M^2},\quad x=\beta X,\quad \omega=\beta\varpi,\quad \kappa_{m\mu}^{\pm}=\frac{\pm\sigma_{m\mu}-\varpi M}{\beta},$$
$$\Omega_{m\mu}^{\pm}=\frac{\mp M\sigma_{m\mu}+\varpi}{\beta},\quad \kappa_{m\mu}+\Omega_{m\mu}M=\pm\beta\sigma_{m\mu},$$

where we can just write $\alpha_{m\mu}$ and $\sigma_{m\mu}$ without left/right distinction, we obtain

$$Q_{m\mu}=\beta\sigma_{m\mu}\left(1-\frac{m^2}{\alpha_{m\mu}^2}\right).$$

So altogether we have for the hollow duct

$$G_m(r,x) = -\frac{\mathrm{e}^{\mathrm{i}M\varpi(X-X_0)}}{2\pi\mathrm{i}\beta}\sum_{\mu=1}^{\infty}\frac{J_m(\alpha_{m\mu}r)J_m(\alpha_{m\mu}r_0)}{\sigma_{m\mu}\left(1-\frac{m^2}{\alpha_{m\mu}^2}\right)J_m^2(\alpha_{m\mu})}\mathrm{e}^{-\mathrm{i}\sigma_{m\mu}|X-X_0|}. \tag{31}$$

Similarly for the annular duct we get

$$G_m(r,x) = -\frac{e^{iM\varpi(X-X_0)}}{2\pi i\beta}\sum_{\mu=1}^{\infty}\frac{\mathscr{C}_m(r;\alpha_{m\mu})\mathscr{C}_m(r_0;\alpha_{m\mu})e^{-i\sigma_{m\mu}|X-X_0|}}{\sigma_{m\mu}\left[\left(1-\frac{m^2}{\alpha_{m\mu}^2}\right)\mathscr{C}_m^2(1;\alpha_{m\mu})-h^2\left(1-\frac{m^2}{\alpha_{m\mu}^2h^2}\right)\mathscr{C}_m^2(h;\alpha_{m\mu})\right]}. \tag{32}$$

Note that apart from the term $\exp[iM\varpi(X-X_0)]$, G_m only depends on M^2 and $|x-x_0|$. Therefore, $|G_m(x,r)|$ is symmetric in $x-x_0$ for any subsonic Mach number.

4. Unstable modes as artifacts of the modelling?

The question of including possible instabilities is not resolved yet. Let us try to summarise our position:

(i) Sound occurs mostly in the form of very small perturbations, and it seems well justified to model it by some form of linearised Euler equations.
(ii) Viscous boundary layers of high-Reynolds flows along walls are, in the aero-engine applications we have in mind, much thinner than a characteristic wave length.
(iii) Points (i) and (ii) together led Ingard [17] and later Myers [18] to derive their impedance wall condition for sound at an impedance wall in a mean flow with slip at the wall (i.e. the boundary layer is collapsed into a vortex sheet [21]). The aero-acoustics community followed them and now the Ingard–Myers boundary condition is the state-of-the-art for this kind of mean flows.
(iv) However, more refined analyses (see Appendix B) as well as numerical time-domain results [13] indicate that the wall vortex sheet along the lined wall may be convectively, or even absolutely [12] unstable. If we blindly followed the model, this would imply that we had to include these instabilities. Maybe this is right for impedances of small resistance with instabilities of small growth rates. For the majority of cases, however, the predicted unstable mode has a large growth rate [10], and we believe that in these cases the instabilities are just artifacts of the model. In physical reality no such instabilities are found [16]. The reason is not clear yet: maybe any instability of the wall vortex sheet is immediately blocked by the wall; maybe the actual wall boundary layer is too thick, cf. Refs. [22,23]; or perhaps our liner-mean-flow model is too simple [12]. In other words: point (ii) is incompatible with point (i).
(v) So we have here three options: (1) include the instability, knowing that the found field is the solution of a questionable model; (2) increase the complexity of the model and thus destroying any possibility of analytical solutions; and (3) ignore, as a "modelling assumption", any instability.

For the examples to be given below, where the growth rates of the candidate instability are very large, we chose option (3).

5. Numerical examples

Numerical evaluation of the pressure field is not too difficult if we are able to find all the modal wavenumbers $\kappa_{m\mu}$ necessary for the required accuracy. We adopted the method, outlined in Ref. [10], which is based on continuation from the (assumed easily found) hard-wall values to the sought soft-wall values. The crux of the method is that we start from a suitable hard-wall direction $|Z|\to\infty$ in the complex impedance plane in order to capture all wavenumbers occurring at the finite impedance, say, Z_0. This is not entirely straightforward. When we trace the wavenumbers backwards, from the soft-wall to the hard-wall values, there are certain intervals of $\arg(Z)$ where some wavenumbers disappear to infinity. These would be impossible to find if we started there with our forward search. It transpires that a search along vertical lines in the complex Z plane, from $Z=\mathrm{Re}(Z_0)-i\infty$ when $M=0$ and from $Z=\mathrm{Re}(Z_0)+i\,\mathrm{sign}(M)\infty$ otherwise, guarantees finding of all the wave numbers.

To be completely specific, we define $Z_0 = R_0 + \mathrm{i}X_0$ and parameterise

$$\frac{1}{Y(\lambda)} = Z(\lambda) = R_0 + \mathrm{i}\delta\ \cot(\lambda), \quad 0 \leqslant \lambda \leqslant \lambda_0 = \operatorname{arccot}(\delta X_0), \tag{33}$$

where $\delta = \operatorname{sign}(M)$ if $M \neq 0$ and $\delta = -1$ if $M = 0$. Solutions κ for the hollow duct are now implicitly given for any λ by the identity

$$f(\kappa, Y) = YE_m(\kappa) = \mathrm{i}\Omega^2 YJ_m(\alpha) + \omega\alpha J'_m(\alpha) \equiv 0. \tag{34}$$

We know the hard-wall solutions corresponding to $\lambda = 0$. After differentiation of f to λ we obtain an ordinary differential equation in κ that can be integrated numerically as an initial value problem. We thus pick a mode by choosing an initial value and solve numerically by standard methods

$$\frac{\mathrm{d}f}{\mathrm{d}\lambda} = \frac{\partial f}{\partial \kappa}\frac{\mathrm{d}\kappa}{\mathrm{d}\lambda} + \frac{\partial f}{\partial Y}\frac{\mathrm{d}Y}{\mathrm{d}\lambda} = 0 \tag{35}$$

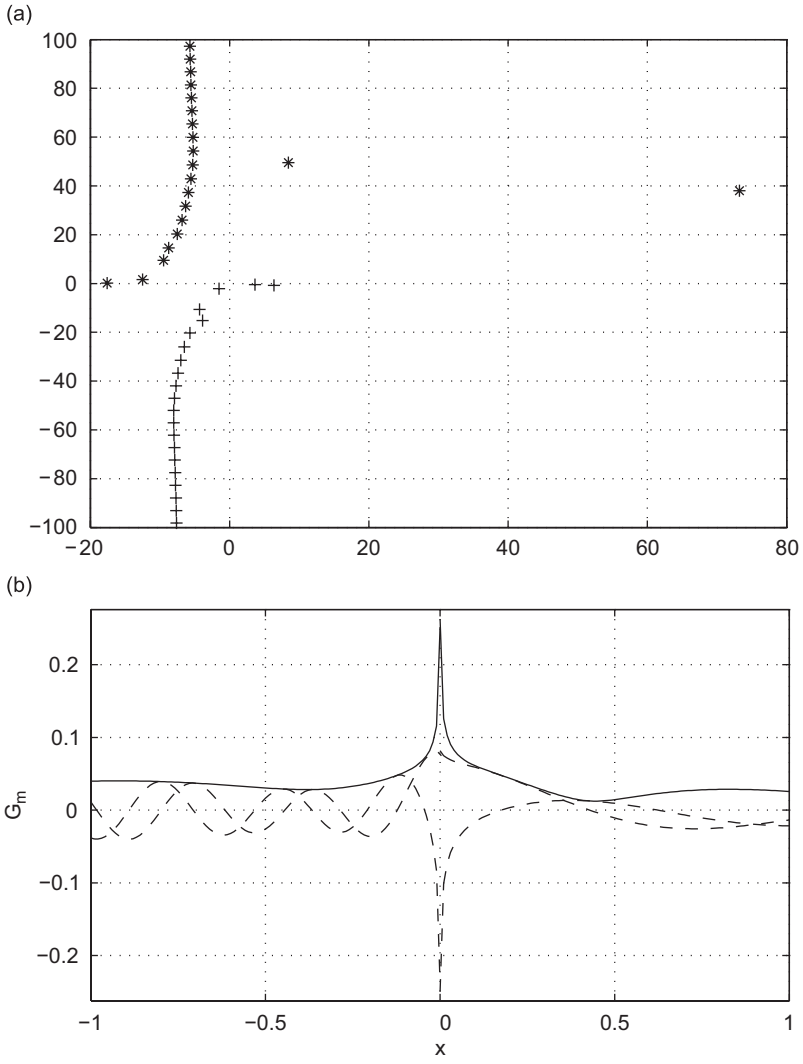

Fig. 2. 400 Modes at $r = r_0 = 0.7$ with $M = 0.5$, $\omega = 10$, $h = 0.3$, $m = 3$, $Z_1 = 1 - \mathrm{i}$, $Z_h = 1 + \mathrm{i}$: (a) complex $\kappa_{m\mu}$-plane; and (b) $\mathrm{Re}(G_m)$ (– –), $\mathrm{Im}(G_m)$ (–·), $|G_m|$ (—).

to obtain an approximation for $\kappa(\lambda_0)$. If we deal with a surface wave, we divide f by J_m. The accuracy of the final result may be optimised by one or two Newton iterations. For an annular duct we do something similar with $f = Y_1 Y_h \mathscr{E}_m$.

The number of terms we need for $G_m(r, x)$ is dependent on the convergence rate, which depends greatly on the value of $x - x_0$. Whenever $x - x_0 \neq 0$ the convergence is exponentially fast, and hence absolute, through the factor $\exp(-\mathrm{i}\kappa_{m\mu}(x - x_0))$. Only when $x = x_0$ the series converges conditionally when $r \neq r_0$, and when $r = r_0$ it diverges (deceivingly) slowly like a harmonic series ($\sim \sum \mu^{-1} \sim \ln(\mu_{\max})$).

As the series at the left and right side of the source plane are not symmetric whenever $M \neq 0$, we will have a discontinuity at $x = x_0$ for any finite number of terms. This jump is a marked evidence of any insufficient accuracy and will disappear when enough terms are included. However, it should be noted that also when M

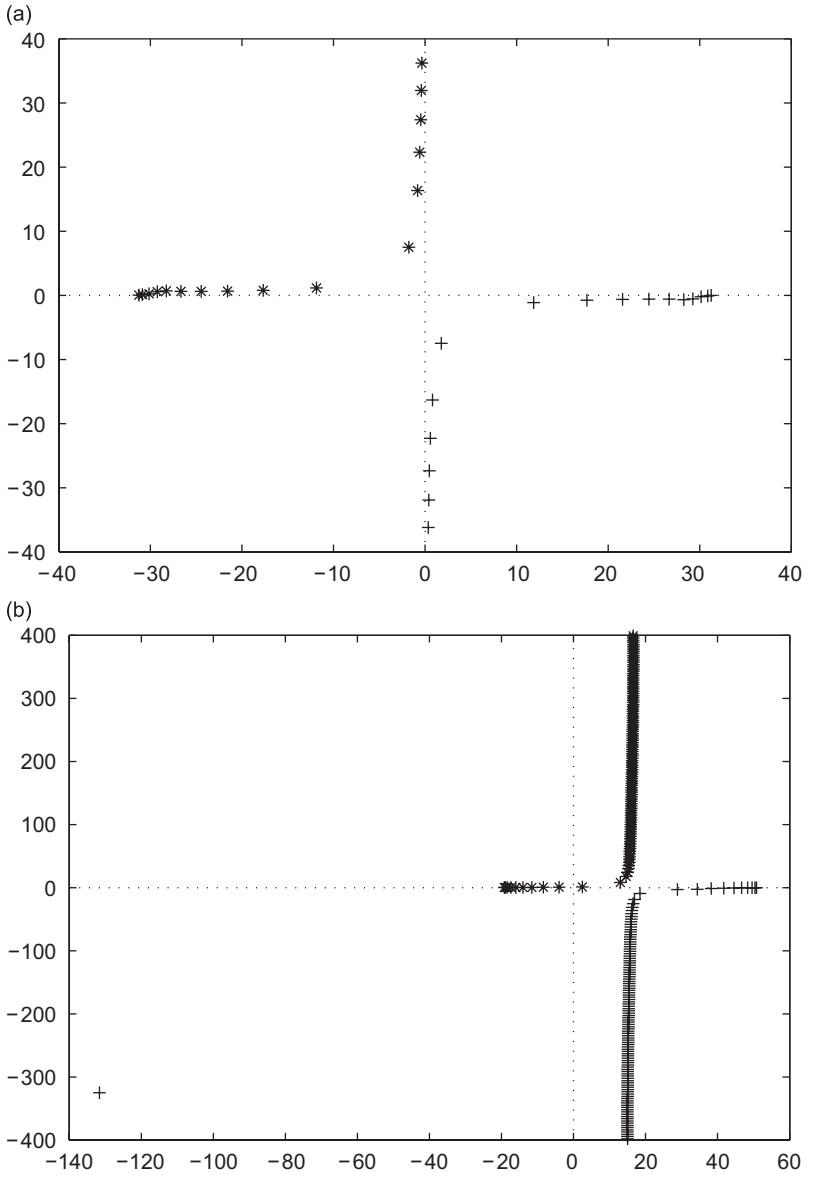

Fig. 3. Location of $\kappa_{m\mu}$ for comparable cases without flow (a) and with flow (b). In both cases is $Z = 2.5$ and $m = 0$, while $\omega = 31.354$ with $M = 0$ (a) and $\omega = 28$ with $M = -0.45$ (b). Note with flow the very well cut-off surface wave, which nevertheless plays a role near the wall around the source plane.

tends to zero the jump will disappear, but only because the solution becomes symmetric. It has no relation to the accuracy of the series.

To illustrate the points noted above, we present the $m = 3$—circumferential component G_m in Fig. 2 for a source at $x_0 = 0$, $r_0 = 0.7$ and $\omega = 10$ in an annular duct with $h = 0.3$, $Z_1 = 1 - \mathrm{i}$ and $Z_h = 1 + \mathrm{i}$ and a mean flow of $M = 0.5$. G_m is plotted at $r = 0.7$ for $-1 \leqslant x \leqslant 1$. In addition the complex axial wave numbers $\kappa_{m\mu}$ are presented. We observe two surface waves in the first quadrant (technically, these are both candidate for instability, but, as indicated above, this fact has no bearing on the present solution). In order to make sure that

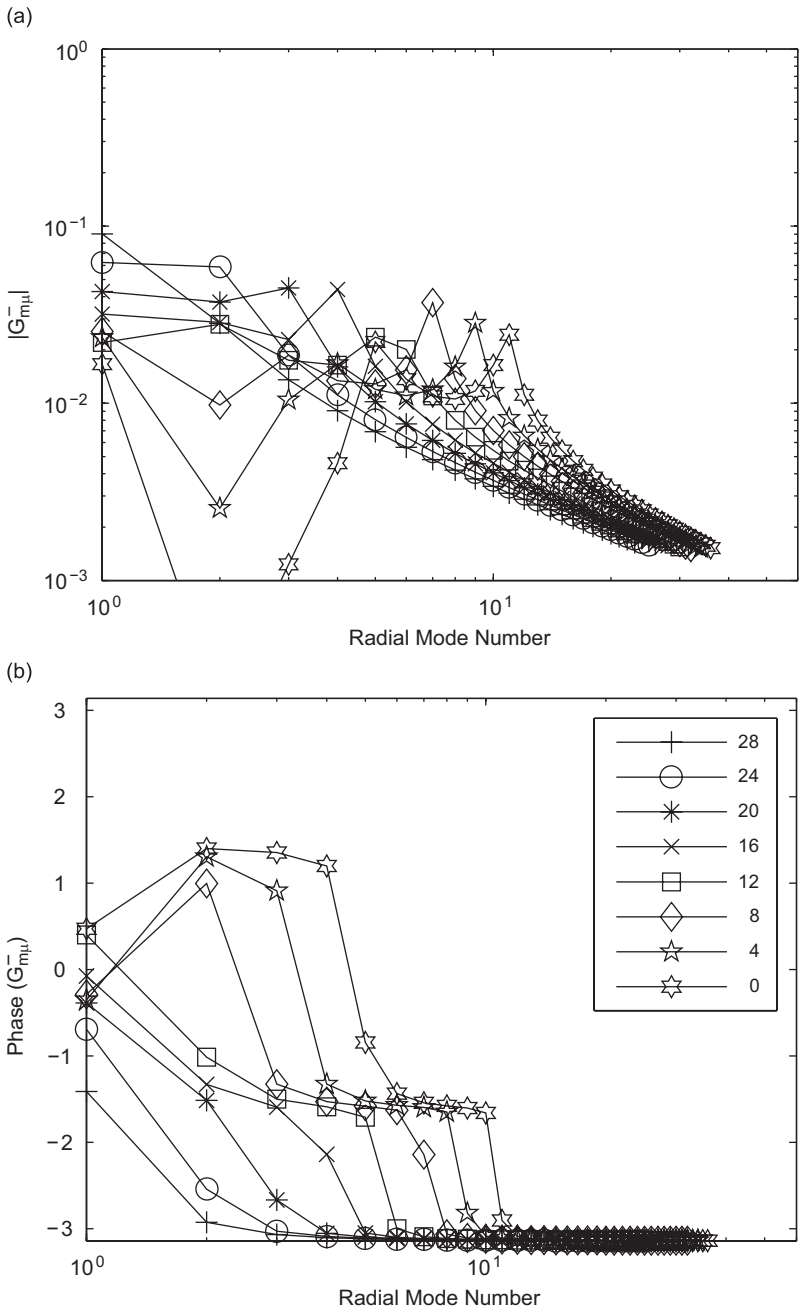

Fig. 4. Green's function mode amplitude: modulus (a) and phase (b) ($\omega = 31.354$, $M = 0$, $Z_1 = 2.5$, $r_0 = 1$, cut-off ratio $= 0.28$). Numerical and analytic results indistinguishable. Left and right running modes the same.

the series has converged in any plotted value of $x \neq x_0$, that is for $400\pi|x - x_0| \gg 1$, say, we used 400 radial modes, but the difference with less than that is only visible very near the source.

In addition to this example for annular ducts we have compared our analytic Green's function for hollow ducts with the 'numerical' Green's function described by Alonso et al. [8]. We consider two cases, one with no mean flow, $M = 0$, and one with a typical 'intake' Mach number of $M = -0.45$. A typical non-dimensional frequency is $\omega = 28$ for the flow case and we choose $\omega = 31.354$ for the zero flow case so that the cut-off ratio of the highest hardwall cut-on mode is about the same for both cases. The impedance is $Z_1 = 2.5 - i0$ in both cases. The number of cut-off modes included in the evaluation of the analytical and numerical Green's function evaluation corresponds to a cut-off ratio of 0.28 (i.e. the number of modes is set equal to the number of modes above that cut-off ratio that would exist if the duct was hard-walled) and only the positive modes in

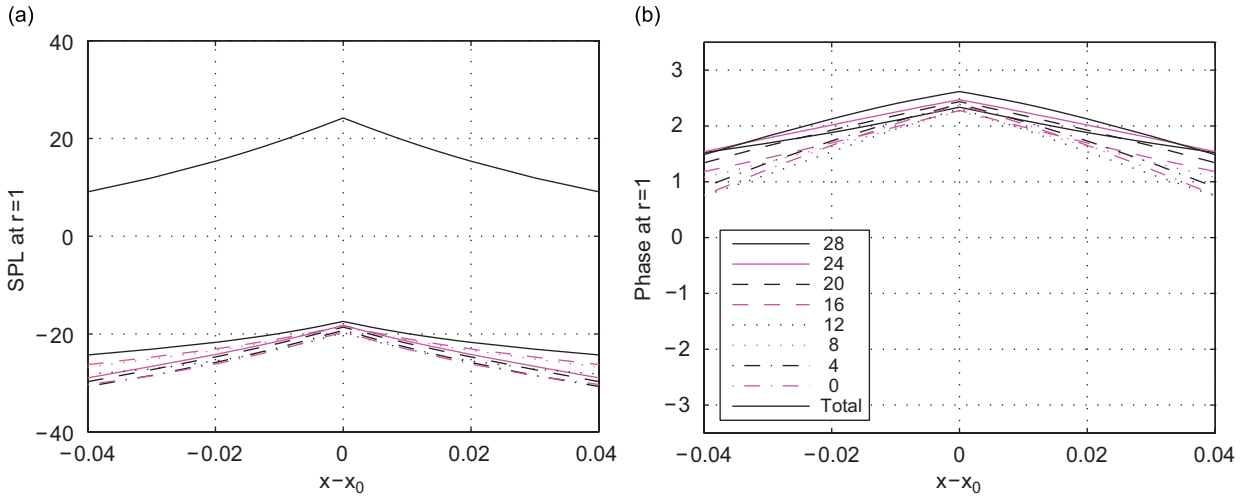

Fig. 5. Axial variation of Green's function amplitudes per azimuthal mode, SPL $= 20\log(|G_m|)$, and total field SPL ($\omega = 31.354$, $M = 0$, $Z_1 = 2.5$, $r_0 = 1$, cut-off ratio $= 0.28$). Numerical and analytic results indistinguishable. Mode amplitude (a) and phase (b) on each side of source plane.

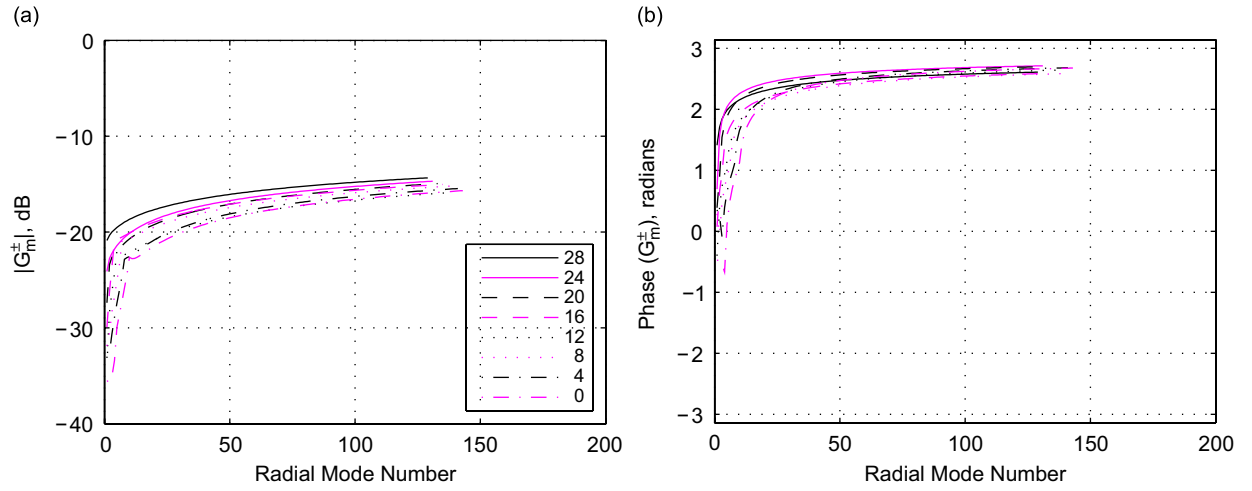

Fig. 6. Analytic Green's function azimuthal mode amplitude variation with increasing radial mode number count μ_{max}; there is no finite asymptotic limit at the source position, as each azimuthal mode amplitude varies like $\log(\mu_{max})$ ($\omega = 31.354$, $M = 0$, $Z_1 = 2.5$, $r_0 = 1$, for min. cut-off ratio of 0.07). Left and right running modes: modulus (a) and phase (b).

the cut-on range 28 (−4) 0 are shown. The source position is always at the wall, $r_0 = 1$, and the observer position is also on the wall, $r = 1$, and at the same azimuthal location as the source but at a variable axial distance from the source both to the left and right of the source plane.

We should explain that this unusual combination of source/observer positions is not particularly relevant to the computation of liner performance—where $x - x_0$ would be typically the liner length for example—but it is relevant to the modelling of liner splice effects and other sources of scattering. Then the liner splice is the "source" of the scattered field and one requires that field in modal form in the direct vicinity of that source.

The typical location of the axial wave numbers in the complex κ-plane for both cases is presented in Figs. 3. The presence of a very well cut-off surface wave in the case with flow anticipates the convergence problems to be reported below when the source is positioned at the wall, right inside the region where the surface wave is important.

For the first (zero flow) case, we show in Fig. 4 the absolute value (or modulus) and corresponding phase of each radial mode amplitude as a function of radial mode number. Each mode is plotted only once, as in this zero-flow case the left and right running modes are the same, while the numerical [8] and analytical results agree to better than 10^{-14}. The same is true for the total field, as illustrated in Fig. 5. Here we have summed the radial modes for each azimuthal mode in the Green's function and plotted the axial variation of each

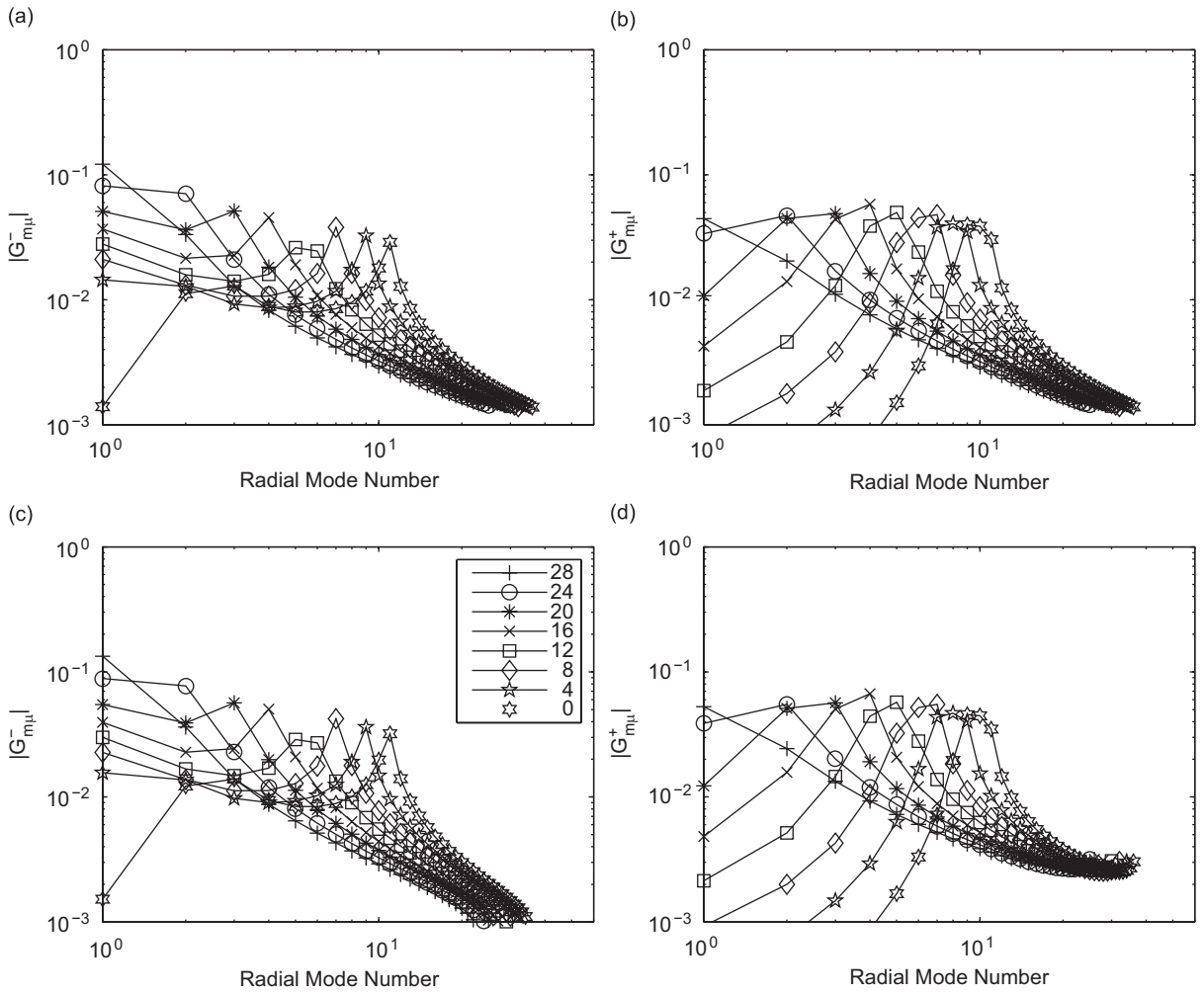

Fig. 7. Analytic v. numerical Green's function mode amplitude: modulus ($\omega = 28$, $M = -0.45$, $Z_1 = 2.5$, $r_0 = 1$, cut-off ratio = 0.28). Analytical: left (a) and right (b) running modes. Numerical: left (c) and right (d) running modes.

azimuthal mode (modulus and phase) for a short distance to the left and right of the source plane, as well as the total Green's function. Although these fields are continuous at the source, this does not mean that we have a converged value at the source plane (maybe near the source). On the contrary, it can be seen (Fig. 6, left) that none of the azimuthal mode amplitudes converge to a finite limit, indeed because the field diverges at the source position $r = r_0$. We cannot demonstrate this as easily with the numerical Green's function, as we have to invert, for each azimuthal mode number, a $2N \times 2N$ matrix where N is the number of radial modes. As we increase N much above 70, depending on the azimuthal mode number, the matrix appears to become ill conditioned and we can no longer solve for the numerical mode amplitudes. However, below that limit the rate of convergence appears to be similar to that of the analytical Green's function.

For the flow case, the picture changes in some ways. In particular, we lose the left/right symmetry for the mode amplitudes, as is seen in Fig. 7. In Fig. 8 we show the ratio of the analytical and numerical mode amplitudes and it can be seen that the two results agree to better than 20% in modulus for the cut-on modes although these differences appear to grow without limit for the very well cut-off modes. As a result the axial variation of the analytical and numerical Green's function agree fairly well away from the source plane, but at and near the source plane there are significant differences, foreshadowing the not yet included surface wave (see below). In particular, Fig. 9 shows that, with this number of modes, the analytical and numerical Green's function have a large but different discontinuity at the source plane.

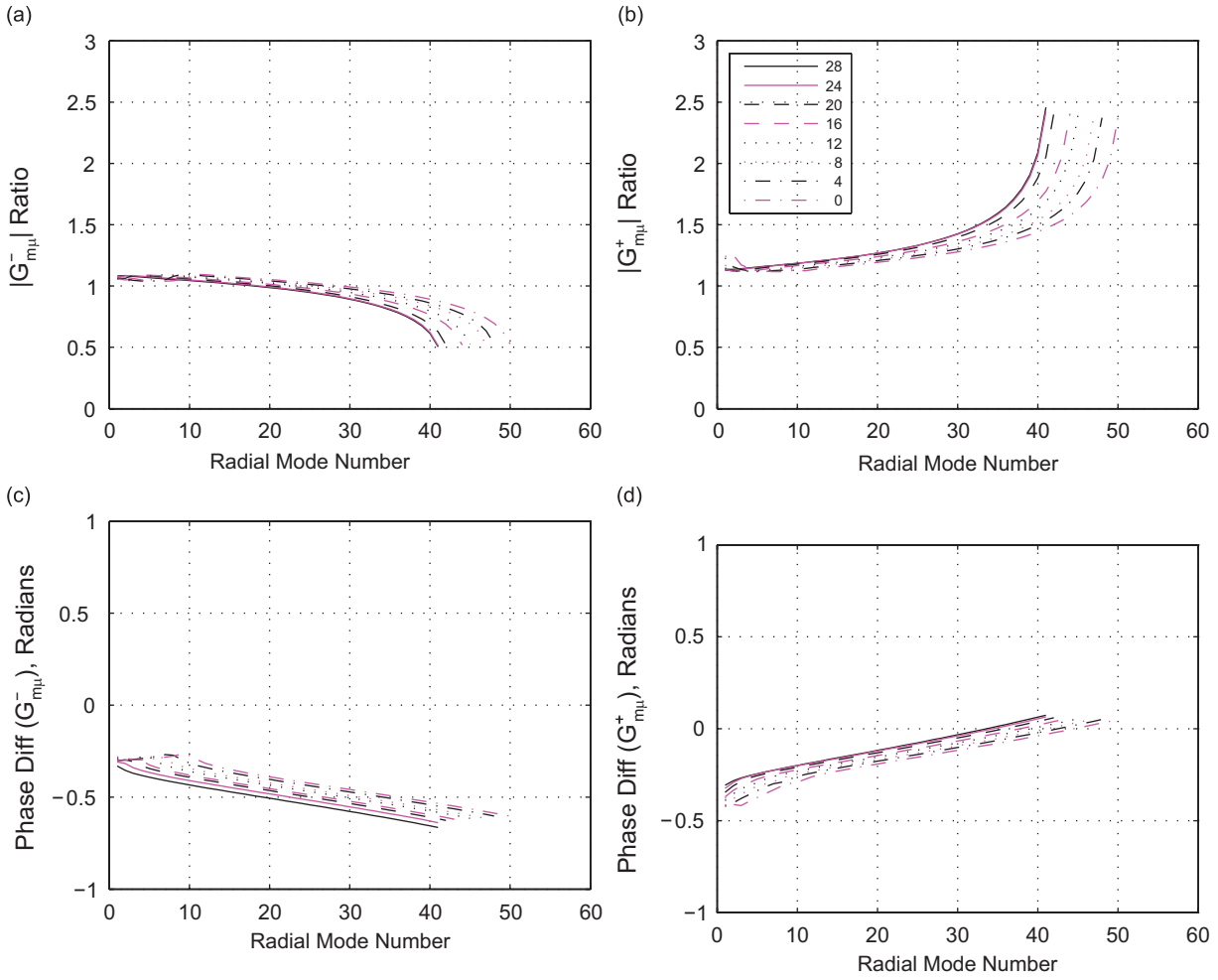

Fig. 8. Ratio of numerical over analytic Green's function mode amplitudes ($\omega = 28$, $M = -0.45$, $Z_1 = 2.5$, $r_0 = 1$; numerical based on 40 cut-off modes). Modulus: left (a) and right (b) running modes. Phase: left (c) and right (d) running modes.

However, with reference to the zero-flow case, if we increase the number of cut-off modes to a cut-off ratio of 0.07, the convergence behaviour is similar in some ways, but strikingly different for the modes to the right of the source plane as shown in Fig. 10. Here there are dramatic jumps in the azimuthal mode amplitudes in the region of radial mode orders 80–95, which has been identified as the effect of a very well cut-off 'surface wave' which makes a large contribution at and near the duct wall (see Fig. 3). Once this has been included, the convergence is similar to the zero flow case. When this high number of radial modes is included in the analytical Green's function, the discontinuity at the source plane disappears as shown in Fig. 11.

The missing surface wave also explains the deviating ratio between analytical and numerical mode amplitudes in Fig. 8. The numerical Green's function with its enforced continuity at the source plane, when evaluated with an insufficient number of cut-off modes, attempts to achieve that continuity by slightly adjusting the amplitude of the cut-on modes and making larger adjustments to the well cut-off modes. When large enough modes are taken, such that any missing surface waves are included, this error will no doubt reduce, but the necessary number of modes may be high (as the present example shows).

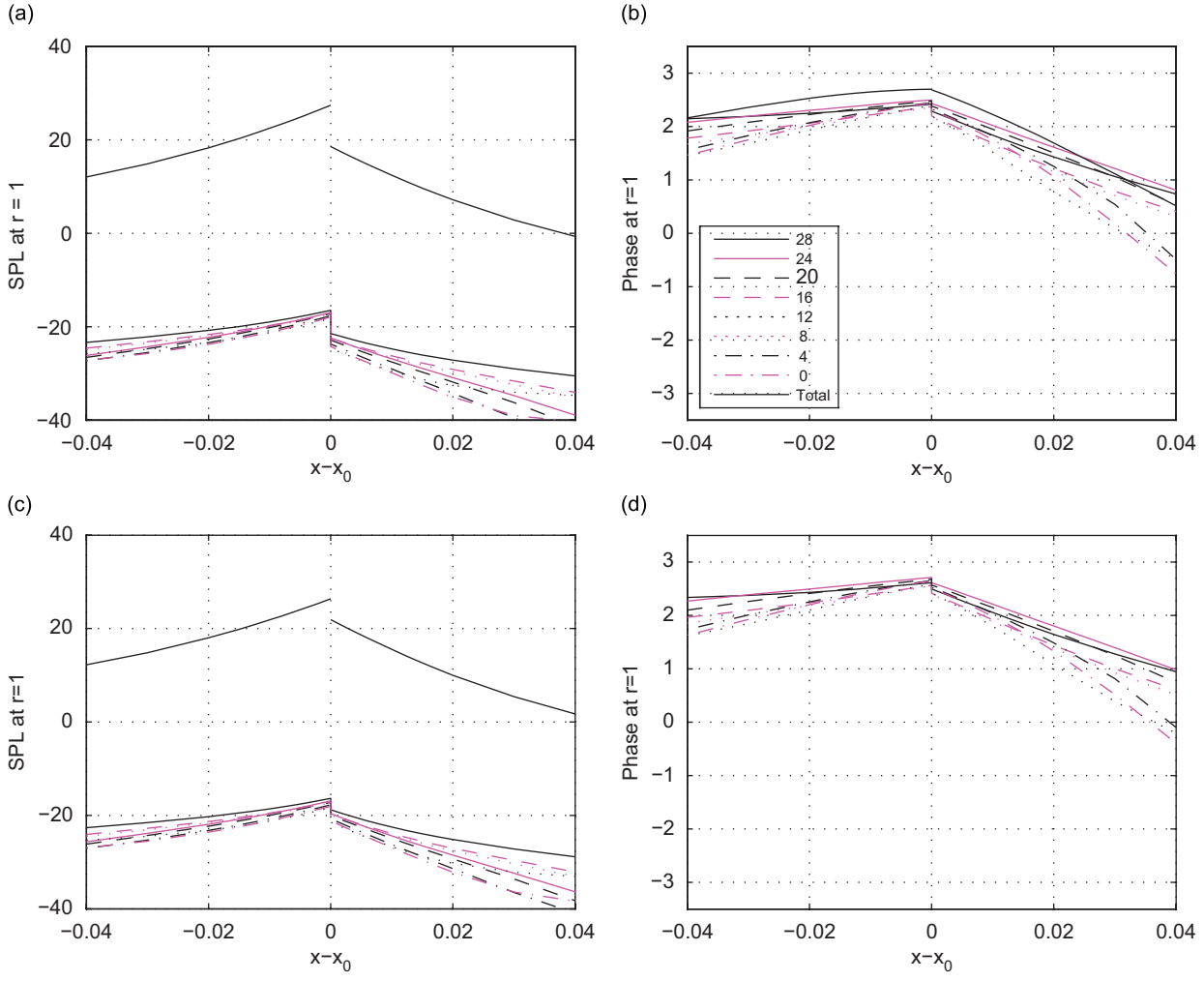

Fig. 9. Axial variation of analytic and numerical Green's function amplitudes per azimuthal mode, SPL $= 20\log(|G_m|)$, and total field SPL ($\omega = 28$, $M = -0.45$, $Z_1 = 2.5$, $r_0 = 1$, cut-off ratio $= 0.28$). Analytical mode amplitude (a) and phase (b), and numerical mode amplitude (c) and phase (d) on each side of source plane.

Finally in order to show the behaviour of the analytical and numerical Green's function continuity at the source plane away from the source position, Fig. 12 for the zero flow case, shows the variation in the *radial* direction at the source plane, at the same azimuthal angle as the source, of the modulus of the azimuthal mode number amplitudes and also the total field, in dB. Shown for comparison is the free-field Green's function $1/(4\pi R)$, where R is the distance from the source at $r_0 = 1$, multiplied by a plane wave correction to account for the reflection or image source in the lined duct wall equal to $2Z_1/(Z_1 + 1)$. It can be seen that the agreement between the analytical and corrected free-field Green's function for this zero flow case is very good and that continuity (i.e. the total field made up of right running modes (+) equals the total field made up of left running modes (−)) at the source plane is achieved away from the source position—these are indistinguishable for this zero flow case. Here we have decreased the cut-off ratio to 0.07 for the analytic Green's function evaluation but had to limit the numerical Green's function evaluation to 40 cut-off radial modes to avoid serious corruption of the solution due to ill-conditioned matrices for the higher azimuthal modes.

The corresponding radial dependence for the mean flow case is shown in Fig. 13. Here we have also used a cut-off ratio of 0.07 for the analytic Green's function evaluation and again 40 cut-off radial modes for the numerical version. This figure shows that we achieved comparable accuracy to the no-flow case in respect of continuity at the source plane and the agreement with the free-field Green's function verifies that we have

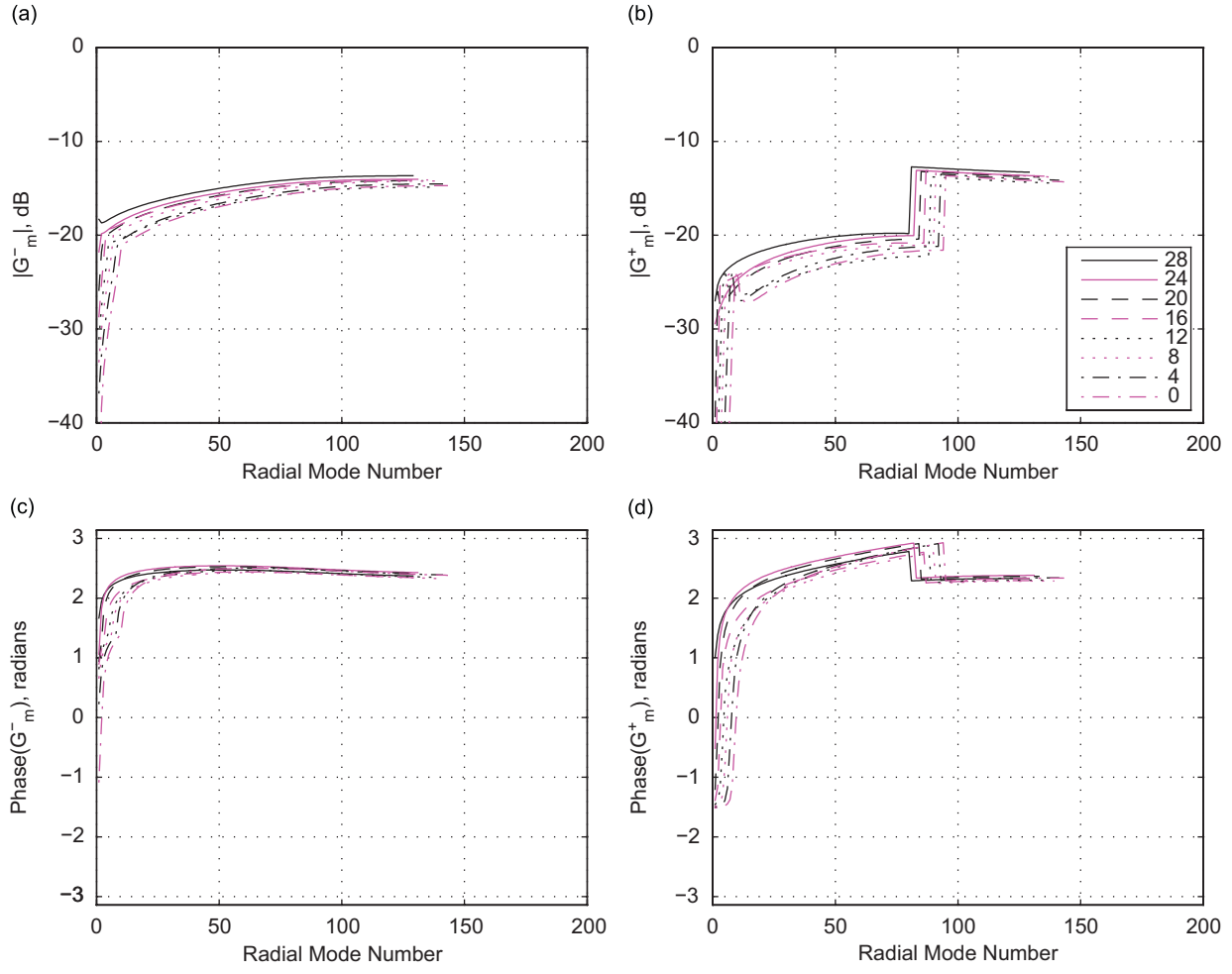

Fig. 10. Analytic Green's function azimuthal mode amplitude convergence ($\omega = 28$, $M = -0.45$, $Z_1 = 2.5$, $r_0 = 1$, cut-off ratio = 0.07). Behaviour of left (a) and right (b) running mode amplitude, left (c) and right (d) running mode phase.

a valid analytical description of the Green's function in the presence of a uniform mean flow. The effects of mean flow on the free-field Green's function have been neglected here as these are small for radiation normal to the mean flow.

6. Conclusions

Since the lined-wall flow-duct modes are not orthogonal, or bi-orthogonal to any convenient set of basis functions, it is not possible to obtain a modal series expansion of the Green's function in the classical way, e.g. as outlined in Ref. [24]. It is possible to set up a linear system for a finite number of amplitudes either by utilising the generalised bi-orthogonality relation of Kraft and Wells [25], or directly as in Alonso and Burdisso [8,9], but the results are approximations, depending on the number of terms. We have followed another approach, by representing the solution as a Fourier integral and converting it into a modal series by summation over the residues. The resulting amplitudes are exact and explicit.

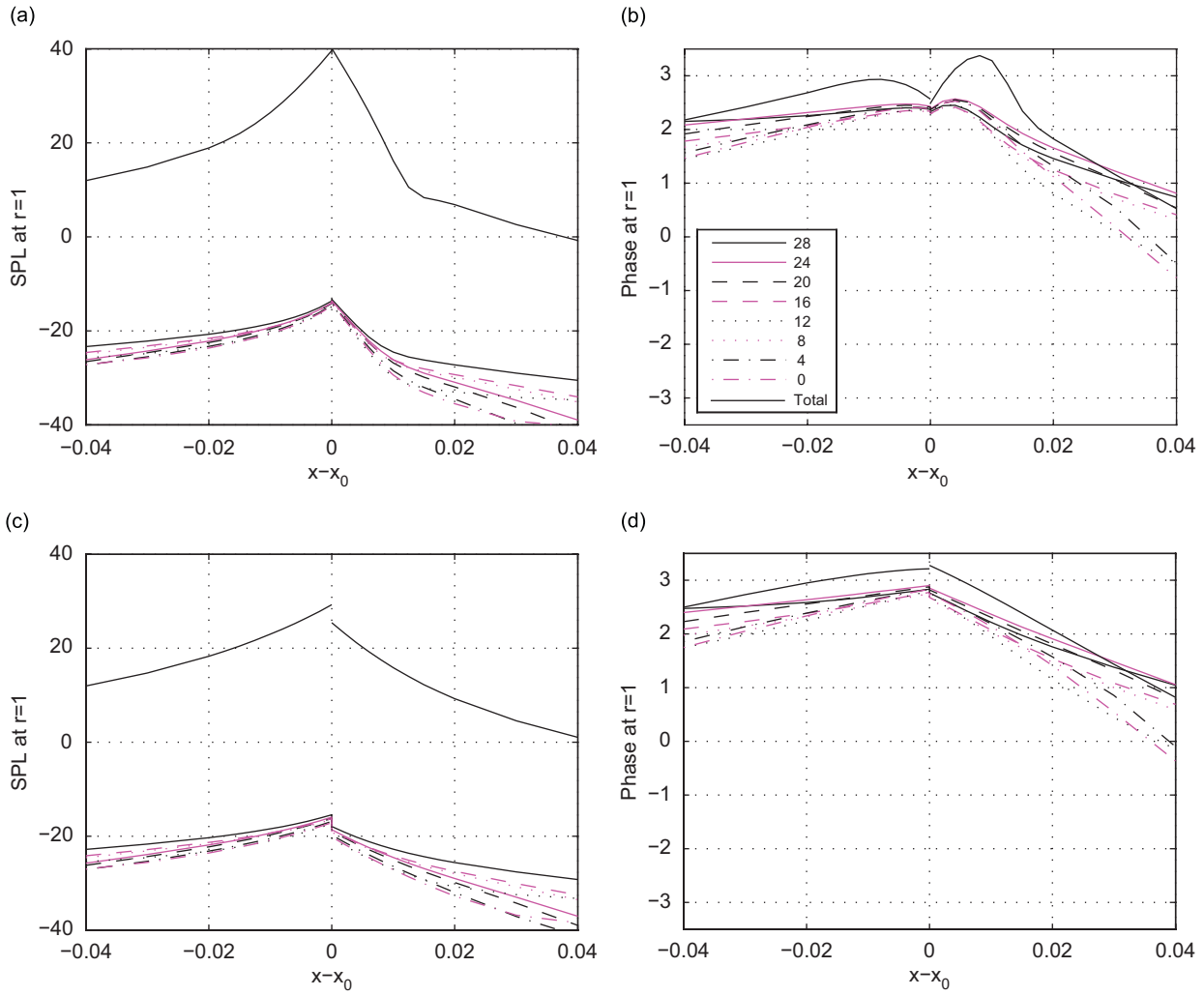

Fig. 11. Axial variation of analytic and numerical Green's function amplitudes per azimuthal mode, SPL $= 20\log(|G_m|)$, and total field SPL ($\omega = 28$, $M = -0.45$, $Z_1 = 2.5$, $r_0 = 1$, analytic: cut-off ratio $= 0.07$, numerical: limited to 40 cut-off modes). Analytical mode amplitude (a) and phase (b), numerical mode amplitude (c) and phase (d) on each side of the source plane.

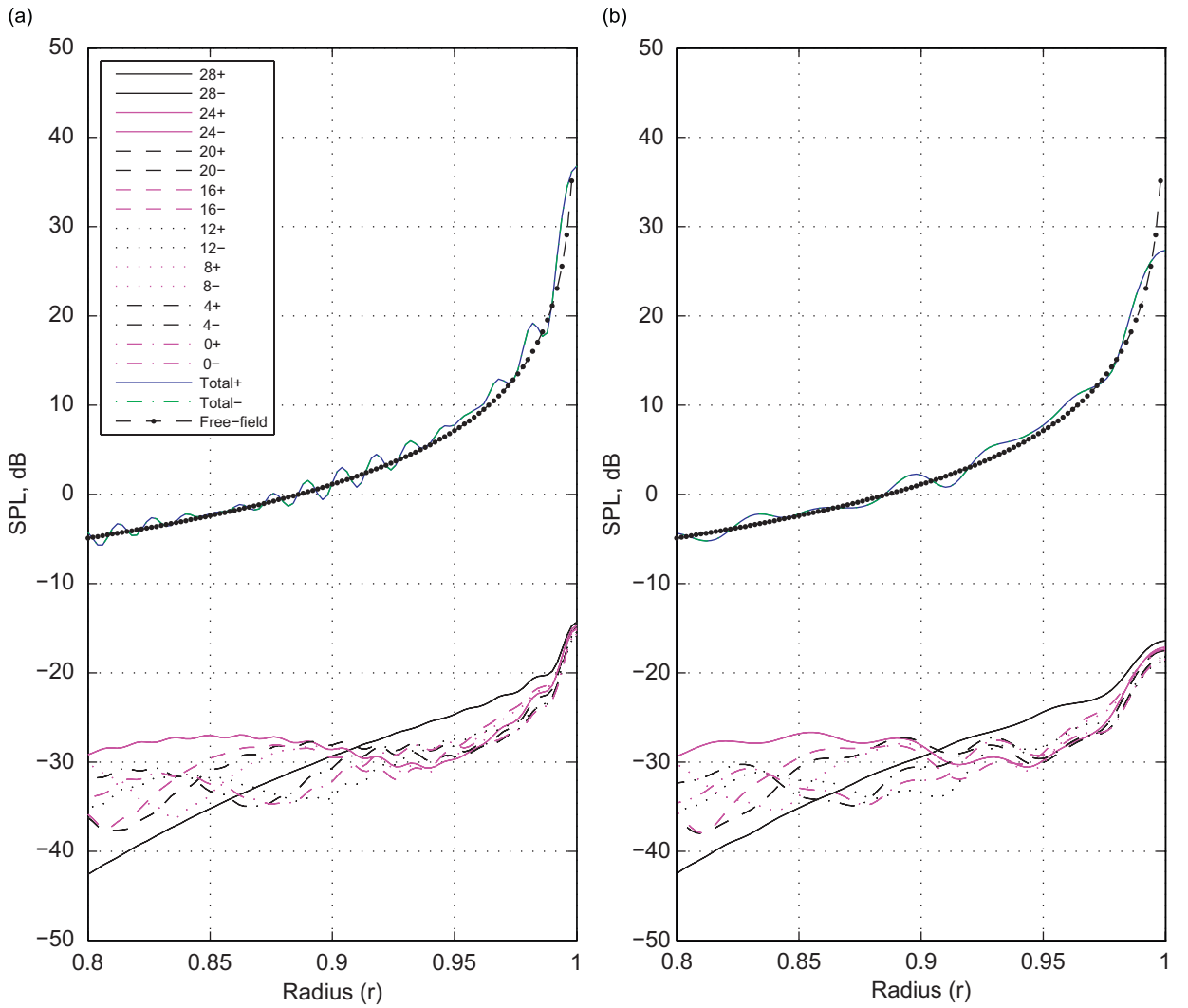

Fig. 12. Radial variation *without flow* of analytic and numerical Green's function amplitudes per azimuthal mode, SPL $= 20\log(|G_m|)$, and total field SPL v. free-field Green's function + reflected SPL ($\omega = 31.354$, $M = 0$, $Z_1 = 2.5$, $r_0 = 1$, analytic: cut-off ratio $= 0.07$, numerical: limited to 40 cut-off modes). Analytical (a), numerical (b). *NB*: The left and right running modal (analytic and numerical) Green's functions, labelled Total+, Total−, are indistinguishable in these no-flow results and oscillate about the *Free-field* Green's function, which decays monotonically away from the source at $r = 1$.

The issue of a possible instability is still an open question. Causality considerations suggest, at least in the linear model, the presence of convective or even absolute instabilities. This has found support by numerical results in time domain [13]. Also experimentally there is evidence [14,15], at least for impedances of small resistance. In most cases, however, the exponentially large fields that would result have little resemblance with physical reality. Therefore, we have not included any such instability in the presented numerical results and adopted stability of the solution as modelling assumption.

Comparison of our analytical mode amplitudes (for the hollow duct version of our solution) with the numerical solution of Alonso et al. showed a good agreement without mean flow, irrespective of how many modes are included in the matrix inversion for the numerical mode amplitudes. A large number of modes are required for convergence near the source. With flow, the mode amplitudes do not agree but as the number of modes included in the matrix inversion is increased, enough to include all important surface

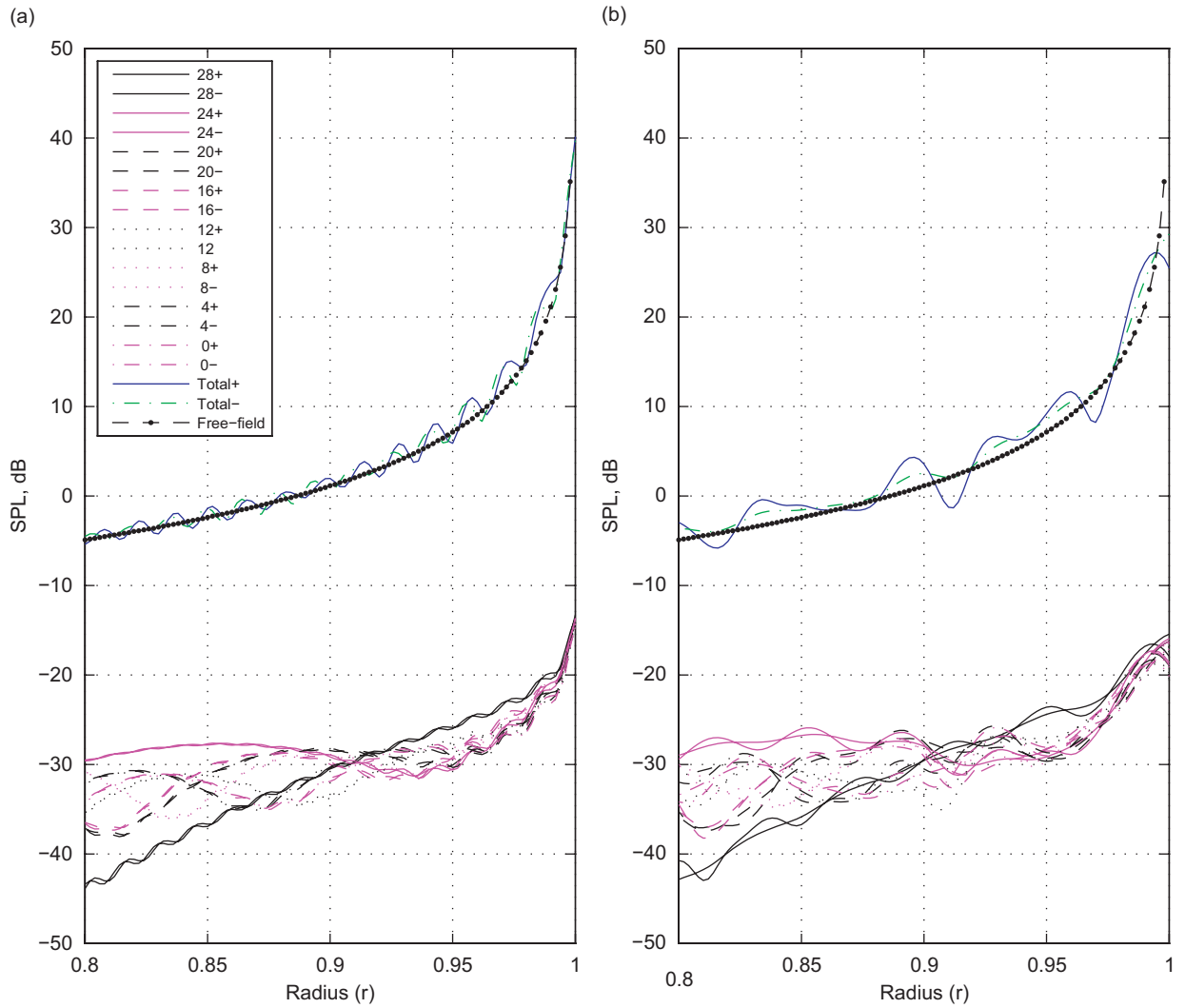

Fig. 13. Radial variation *with flow* of analytic and numerical Green's function amplitudes per azimuthal mode, SPL $= 20\log(|G_m|)$, and total field SPL v. free-field Green's function + reflected SPL ($\omega = 28$, $M = -0.45$, $Z_1 = 2.5$, $r_0 = 1$, analytic: cut-off ratio $= 0.07$, numerical: limited to 40 cut-off modes). Analytical (a), numerical (b).
NB: The left and right running analytic modal Green's functions, labelled Total+, Total−, can just be distinguished in these with-flow results and more so for the numerical Green's function, both oscillating about the monotonic *Free-field* Green's function.

waves, the numerically obtained modal amplitudes of Alonso et al. appear to be converging to the present analytical result.

Indeed, this numerical exercise showed the importance of including all relevant modes, especially when they behave as surface waves. When source and observer position are at the wall, they are in the regime of the surface wave, so irrespective of the modal decay rate, overlooking the surface wave produces an unconverged solution and a detectable discontinuity of the field at the source. A reliable method to find all modes, based on their behaviour with impedance Z along lines parallel to the imaginary axis is described in some detail.

In practical applications our closed form analytic Green's function will be computationally more efficient, especially at high frequencies of practical interest to aero-engine applications, and the analytic form for the mode amplitudes could permit future modelling advances not possible from the numerical equivalent. For example it has already been applied to post-processing of phased array measurements inside lined ducts by Sijtsma [26].

Acknowledgements

The contribution of SWR was partly carried out during a visit of the Department of Applied Mathematics and Theoretical Physics of the University of Cambridge, financed by a grant from the Royal Society, in the Spring of 2004. We are very grateful to both the Royal Society, the Department and Professor Nigel Peake for their support, hospitality, inspiring discussions and interest.

We acknowledge the discussions with Ed Brambley (DAMTP, Cambridge University).

We are grateful to ms dr Heike JJ Gramberg and dr Nick C Ovenden for skillfully implementing the routine (34) to find all modal wave numbers. The present results would not have been possible without it.

Appendix A. Corrected form of Tester et al. [1]

Unfortunately, Eq. (2) of Tester et al. [1] contains some minor typographical errors. The corrected form is given by

$$G(x,r,\theta|x_0,r_0,\theta_0) = -\frac{1}{2\pi \mathrm{i}}\sum_{m,n}\frac{J_m(k^{\pm}_{rmn}r)J_m(k^{\pm}_{rmn}r_0)}{\chi^{\pm}_{mn}\Lambda^{\pm}_{mn}}\exp[-\mathrm{i}k^{\pm}_{xmn}|x-x_0|]\exp[-\mathrm{i}m(\theta-\theta_0)],$$

where $k^{\pm}_{xmn} = (\mp M_x k + \chi^{\pm}_{mn})/(1-M_x^2)$, $\chi^{\pm}_{mn} = (k^2-(1-M_x^2)k^{\pm 2}_{rmn})^{1/2}$ with $\mathrm{Im}(\chi_{mn})\leqslant 0$, and

$$\Lambda^{\pm}_{mn} = J'_m(k^{\pm}_{rmn})^2 + J_m(k^{\pm}_{rmn})^2\left[1-\frac{m^2}{k^{\pm 2}_{rmn}} \mp \frac{2\mathrm{i}M_x(1\mp k^{\pm}_{xmn}M_x/k)}{Z\chi^{\pm}_{mn}}\right].$$

This is equivalent to the present form if we identify $\omega = k$, $\alpha_{m\mu} = k_{rmn}$, $\kappa_{m\mu} = \pm k_{xmn}$, $(\kappa_{m\mu}+\Omega_{m\mu}M) = \pm\chi_{mn}$ and $Q_{m\mu}J_m(\alpha_{m\mu})^2 = \chi_{mn}\Lambda_{mn}$, with the understanding that the upper sign is taken for the $x>x_0$ (i.e. the right running modes) and the lower sign for $x<x_0$ (i.e. the left running modes). This notation has the advantage that the reciprocity rule is more obvious, that is, if we exchange the observer position for the source position, the modes are the same as those we would use by simply reversing the sign of the Mach number in the above equations.

Appendix B. Causality

From analogy with the Helmholtz instability along an interface between two media of different velocities, Tester [4] put forward the possibility that some modes may have the character of a convective instability. This means that the mode seems to propagate in the upstream direction while it decays exponentially, but in reality its direction of propagation is downstream and it increases exponentially.

In the following we will indicate a possible way to recognise these convectively unstable modes. It should be noted that we assume here only the possibility of convective instabilities with a field of the same time-harmonic behaviour as the exciting source, i.e. $\sim \mathrm{e}^{\mathrm{i}\omega t}$ where ω is real. If the system is really absolutely unstable [12], this assumption does not hold out.

To determine the direction of propagation of the duct modes we have available the causality criterion of Briggs–Bers [27–29], where analyticity in the whole lower complex ω-plane is enforced by tracing the poles for fixed $\mathrm{Re}(\omega)$, and $\mathrm{Im}(\omega)$ running from 0 to $-\infty$. Unfortunately, this criterion is not applicable to vortex sheet-type instabilities as it requires the system to have a maximum temporal growth rate for all real wave numbers. With vortex sheet instabilities the growth rate is not bounded since the axial wave number is asymptotically linearly proportional to the frequency.

Therefore, we will fall back on the Crighton–Leppington [11,30,31] test, to trace the poles for fixed $|\omega|$, and $\arg(\omega)$ running from 0 to $-\frac{1}{2}\pi$, and check to see if they cross the real axis and change their halfplanes. This test was originally devised for a pure vortex sheet Helmholtz instability without other length scales involved than the acoustic wave length. In this case it is sufficient to rotate ω to the imaginary axis. If the situation is more complex, involving other length scales, ω may have to be increased first [12].

Fig. 14 shows the behaviour of axial wave numbers $\kappa_{m\mu}$ for complex ω, with impedance model $Z(\omega) = R + \mathrm{i}a\omega - \mathrm{i}b/\omega$. This Z is chosen such that it is physical ($Z(\omega) = Z^*(-\omega)$), causal (Z is analytic and non-zero in $\mathrm{Im}(\omega)<0$), and passive ($\mathrm{Re}(Z)>0$). See e.g. Refs. [32,33].

One mode crosses the real κ-axis, suggesting that the integration contour of the inverse Fourier transform should to be taken as given in Fig. 15. In other words, this mode is to be counted among the right-running modes of the lower half-plane. The results after assembling the residue contributions from below the contour for $x>x_0$ and from above the contour for $x<x_0$ are exactly the same in form as given by Eqs. (20) and (30).

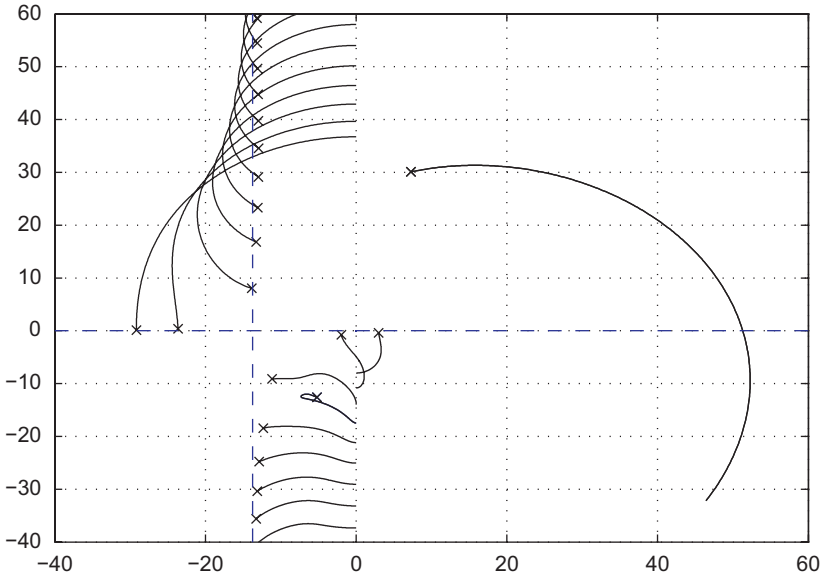

Fig. 14. Causality contours by tracing complex $\omega = |\omega|\mathrm{e}^{-\mathrm{i}\varphi}$ in complex plane. The crosses indicate the location of the modes when $\mathrm{Im}(\omega) = 0$ ($Z = 1 + 1.385\mathrm{i}$, $\omega = 10$, $M = 0.7$, $m = 5$, $a = 0.15$, $b = 1.15$).

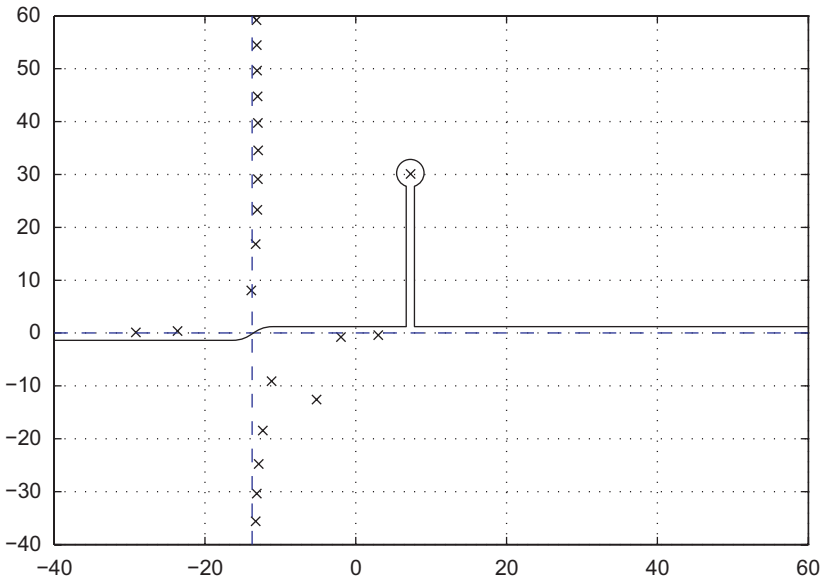

Fig. 15. The deformed integration contour capturing the instability ($Z = 1 + 1.385\mathrm{i}$, $\omega = 10$, $M = 0.7$, $m = 5$, $a = 0.15$, $b = 1.15$).

So we have (with $M>0$) for the hollow duct

$$G_m(r,x)=\begin{cases}\sum_{\mu=1}^{\infty'} G^-_{m\mu}(r)\mathrm{e}^{-\mathrm{i}\kappa^-_{m\mu}(x-x_0)} & \text{if } x<x_0,\\ \sum_{\mu=1}^{\infty} G^+_{m\mu}(r)\mathrm{e}^{-\mathrm{i}\kappa^+_{m\mu}(x-x_0)}+G^-_{m\mu_1}(r)\mathrm{e}^{-\mathrm{i}\kappa^-_{m\mu_1}(x-x_0)} & \text{if } x>x_0,\end{cases} \tag{B.1}$$

and for the annular duct

$$G_m(r,x)=\begin{cases}\sum_{\mu=1}^{\infty''} G^-_{m\mu}(r)\mathrm{e}^{-\mathrm{i}\kappa^-_{m\mu}(x-x_0)} & \text{if } x<x_0,\\ \sum_{\mu=1}^{\infty} G^+_{m\mu}(r)\mathrm{e}^{-\mathrm{i}\kappa^+_{m\mu}(x-x_0)} & \\ \quad +G^-_{m\mu_1}(r)\mathrm{e}^{-\mathrm{i}\kappa^-_{m\mu_1}(x-x_0)}+G^-_{m\mu_2}(r)\mathrm{e}^{-\mathrm{i}\kappa^-_{m\mu_2}(x-x_0)} & \text{if } x>x_0,\end{cases} \tag{B.2}$$

where we adopted the following notation: the modes with their axial wave numbers in the lower, upper complex half plane are indicated by a $+$, $-$ superscript, the unstable modes are denoted by $\mu=\mu_1$ (for the hollow duct) or $\mu=\mu_1$ and μ_2 for the annular duct, and $\sum'$ or $\sum''$ denote that in the summation the μ_1-th or the μ_1-th and μ_2-th terms are skipped. Note that whether we satisfy causality or simply interpret the unstable mode as an upstream decaying mode, $G_m(r,x)$ is continuous at $x=x_0$ although its value differs of course.

References

[1] B.J. Tester, N.J. Baker, A.J. Kempton, M.C.M. Wright, Validation of an analytical model for scattering by intake liner splices, AIAA 2004–2906, *10th AIAA/CEAS Aeroacoustic Conference*, Manchester, UK, 2004.

[2] B.J. Tester, C.J. Powles, N.J. Baker, A.J. Kempton, Scattering of sound by liner splices: a Kirchhoff model with numerical verification, *AIAA Journal* 44 (9) (2006) 2009–2017.

[3] A.M. Cargill, *Rolls-Royce Internal Report TSG0688*, 1993.

[4] B.J. Tester, The propagation and attenuation of sound in ducts containing uniform or "plug" flow, *Journal of Sound and Vibration* 28 (2) (1973) 151–203.

[5] M.A. Swinbanks, The sound field generated by a source distribution in a long duct carrying sheared flow, *Journal of Sound and Vibration* 40 (1) (1975) 51–76.

[6] J.B.H.M. Schulten, *Sound Generation by Ducted Fans and Propellers as a Lifting Surface Problem*, Ph.D. Thesis, University of Twente, Enschede, The Netherlands, 1993.

[7] W.E. Zorumski, *Acoustic Theory of Axisymmetric Multisectioned Ducts*, NASA TR R-419, 1974.

[8] J.S. Alonso, R.A. Burdisso, Sound radiation from the boundary in a circular lined duct with flow, AIAA 2003–3144, *Ninth AIAA/CEAS Aeroacoustic Conference*, Hilton Head, USA, 2003.

[9] J.S. Alonso, L.R. Molisani, R.A. Burdisso, Spectral and wavenumber approaches to obtain Green's functions for the convected wave equation, AIAA 2004–2943, *10th AIAA/CEAS Aeroacoustic Conference*, Manchester, UK, 2004.

[10] S.W. Rienstra, A classification of duct modes based on surface waves, *Wave Motion* 37 (2) (2003) 119–135.

[11] S.W. Rienstra, Acoustic scattering at a hard–soft lining transition in a flow duct, *Journal of Engineering Mathematics* 59 (4) (2007).

[12] E.J. Brambley, N. Peake, Surface-waves, stability, and scattering for a lined duct with flow, AIAA 2006–2688, *12th AIAA/CEAS Aeroacoustics Conference*, Cambridge, MA, 8–10 May 2006.

[13] N. Chevaugeon, J.-F. Remacle, X. Gallez, Discontinuous Galerkin implementation of the extended Helmholtz resonator impedance model in time domain, AIAA 2006–2569, *12th AIAA/CEAS Aeroacoustics Conference*, Cambridge, MA, 8–10 May 2006.

[14] M. Brandes, D. Ronneberger, Sound amplification in flow ducts lined with a periodic sequence of resonators, AIAA paper 95–126, *First AIAA/CEAS Aeroacoustics Conference*, Munich, Germany, 12–15 June 1995.

[15] Y. Aurégan, M. Leroux, V. Pagneux, Abnormal behavior of an acoustical liner with flow, *Forum Acusticum 2005*, Budapest, 2005.

[16] H.H. Hubbard, *Aeroacoustics of Flight Vehicles: Theory and Practice. Volume 2: Noise Control*, Acoustical Society of America, Woodbury, NY, 1995.

[17] K.U. Ingard, Influence of fluid motion past a plane boundary on sound reflection, absorption, and transmission, *Journal of the Acoustical Society of America* 31 (7) (1959) 1035–1036.

[18] M.K. Myers, On the acoustic boundary condition in the presence of flow, *Journal of Sound and Vibration* 71 (3) (1980) 429–434.

[19] M. Abramowitz, I.A. Stegun, *Handbook of Mathematical Functions, National Bureau of Standards*, Dover Publications Inc., New York, 1964.

[20] W. Koch, W. Möhring, Eigensolutions for liners in uniform mean flow ducts, *AIAA Journal* 21 (1983) 200–213.

[21] W. Eversman, R.J. Beckemeyer, Transmission of sound in ducts with thin shear layers—convergence to the uniform flow case, *The Journal of the Acoustical Society of America* 52 (1) (1972) 216–220.
[22] A. Michalke, On spatially growing disturbances in an inviscid shear layer, *Journal of Fluid Mechanics* 23 (3) (1965) 521–544.
[23] A. Michalke, Survey on jet instability theory, *Progress in Aerospace Science* 21 (1984) 159–199.
[24] G.F. Roach, *Green's Functions*, Cambridge University Press, Cambridge, 1982.
[25] R.E. Kraft, W.R. Wells, Adjointness properties for differential systems with eigenvalue-dependent boundary conditions, with application to flow-duct acoustics, *The Journal of the Acoustical Society of America* 61 (4) (1977) 913–922.
[26] P. Sijtsma, Feasibility of in-duct beamforming, AIAA 2007–3696, *13th AIAA/CEAS Aeroacoustics Conference*, Rome, Italy, 21–23 May 2007.
[27] A. Bers, R.J. Briggs, *MIT Research Laboratory of Electronics Report no. 71*, unpublished, 1963.
[28] R.J. Briggs, *Electron-Stream Interaction with Plasmas*, Monograph no. 29, MIT Press, Cambridge, MA, 1964.
[29] A. Bers, Space-time evolution of plasma instabilities—absolute and convective, in: M.N. Rosenbluth, R.Z. Sagdeev (Eds.), *Handbook of Plasma Physics*, Vol. I, North-Holland, Amsterdam, 1983, p. 451.
[30] D.G. Crighton, F.G. Leppington, Radiation properties of the semi-infinite vortex sheet: the initial-value problem, *Journal of Fluid Mechanics* 64 (2) (1974) 393–414.
[31] D.S. Jones, J.D. Morgan, The instability of a vortex sheet on a subsonic stream under acoustic radiation, *Proceedings of the Cambridge Philosophical Society Mathematical and Physical Sciences*, Vol. 72, 1972, pp. 465–488.
[32] S.W. Rienstra, 1D reflection at an impedance wall, *Journal of Sound and Vibration* 125 (1988) 43–51.
[33] S.W. Rienstra, Impedance models in time domain, including the extended Helmholtz resonator model, AIAA 2006–2686, *12th AIAA/CEAS Aeroacoustics Conference*, Cambridge, MA, USA, 8–10 May 2006.